Commun. Comput. Chem. Vol.**2**, No.**2**, pp.88-100
doi: 10.4208/cicc.2014.v2.n2.5 June 2014

REGULAR ARTICLE

A DFT/TDDFT Study on the Luminescence Property and Adsorption Behaviors of a Luminescence MOFs as a Potential Probe for Detecting Formaldehyde

Shuhe Kang, Zhiqiao Liu, Jiaojie Tan, Ce Hao* and Jieshan Qiu

State Key Laboratory of Fine Chemicals, Dalian University of Technology, Dalian 116024, Liaoning, China

Received 23 April 2014; Accepted (in revised version) 27 May 2014

Abstract: Density Functional Theory (DFT) and Time-Dependent Density Functional Theory (TDDFT) have been carried out to investigate luminescence property and adsorption behaviors of the MOFs, $Zn_3(BTC)_2(DMF)_3(H_2O)\bullet(DMF)(H_2O)$. Through the analysis of the binding energy and hydrogen bond complexes' structure, we proved that the MOFs can absorb formaldehyde and other small molecules. We pointed out that the luminescence mechanism of the MOFs is ligand-based luminescence by the analysis of frontier molecular orbitals (FMOs) and the corresponding electronic configurations of the MOFs and its hydrogen bond complexes. But when the CH_2O hydrogen bond complex is formed, the luminescence mechanism will change into dominating by the guest-induced luminescence. Accordingly, the MOFs have good potential for detecting formaldehyde in environment

AMS subject classifications: 74E70,78M50
Keywords: DFT, TDDFT, MOFs, luminescence, adsorption

1. Introduction

Metal-Organic Frameworks (MOFs), a new fascinating class of porous materials, are synthesized via self-assembly with metal centers or clusters and organic linkers to form

* Corresponding author. *Email address*: haoce @dlut.edu.cn (C. Hao)

crystalline networks [1-3]. MOFs have an essentially infinite number of possible combinations of metal ions, organic linkers, and structural motifs, so MOFs exhibit extraordinary optoelectronic, ferroelectric, magnetic, adsorption, catalytic and luminescence properties [4-11]. In recent years, MOFs have attracted considerable interests for applications in a number of fields, especially in gas adsorption and Chemical Sensing [10-12].

Formaldehyde is widely used in construction such as wood processing, furniture, textiles, and carpeting [13], the effects of formaldehyde on human health have attracted great attention [14-17]. The conventional formaldehyde measurement systems are expensive and bulky, so a better one should be developed [18]. MOFs contain many hydrogen bond donors and acceptors, so formaldehyde will be adsorbed in MOFs by forming hydrogen bond complexes. Hydrogen bond plays an important role in many photophysical processes and photochemical reactions in the electronic excited state [19-33]. Luminescence properties of MOFs may be changed by absorbing formaldehyde, and therefore MOFs can be used as chemical sensor for detecting formaldehyde.

In 2006, a 3D chiral microporous MOFs, $Zn_3(BTC)_2(DMF)_3(H_2O)\bullet(DMF)(H_2O)$, was synthesized by Fang et al.. The solid-state excitation-emission spectra showed that the strongest excitation peaks is at 341 nm, and its emission spectra mainly showed strong peaks at 410 nm [34]. The MOFs also exhibit substantial adsorption behaviors for H_2O, CH_3OH and C_2H_5OH [34]. Due to the excellent luminescence property and good adsorption behaviors, the MOFs will be a potential chemical sensor for small molecules. In this work, we investigated the luminescence property and adsorption behaviors of the MOFs by using Density Functional Theory (DFT) and Time-Dependent Density Functional Theory (TDDFT). At first, We have intercepted the representative segment A ($Zn_2L_4(DMF)_2$，where L is benzoic acid) to study ground state geometric structure and excited energy of the MOFs. Furthermore, we considered hydrogen bond complexes which were formed by small molecules (H_2O, CH_3OH, C_2H_5OH and CH_2O) and A to study adsorption behaviors and luminescence properties of the MOFs. Through the analysis of the results, we predicted the possibility of using the MOFs as Luminescence-Based Chemical Sensor for detecting small molecules. In particular, we had more interesting in detecting formaldehyde in environment.

2. Computational details

MOFs are periodic crystalline material periodic structures. To avoid the complexity of periodic structures in the excited state, we truncated the $Zn_3(BTC)_2(DMF)_3(H_2O)\bullet(DMF)(H_2O)$ crystal structure into a representative segment A (see **Figure 1**). DFT and TDDFT were employed for ground state and excited state computations, respectively. The ground state and excited state computations of A was performed by using

the Generalized Gradient Approximation (GGA) with Perdew-Burke-Ernzerhofer (PBE) exchange-correlation functional and the Becke's three parameter hybrid exchange functional with Lee-Yang-Parr (B3LYP) gradient corrected correlation functional in the Turbomole 6.4 program package, TZVP basis set was used for all of atoms [35-38]. We also used the long-range corrected version of B3LYP (CAM-B3LYP) by Handy and coworkers in the Gaussian 09 program package and the LANL2DZ basis set for Zn atoms and 6-31+G(d,p) basis set for remaining atoms [39-40]. As the results of section 3.1, we selected the PBE/TZVP level to perform the following DFT and TDDFT calculation.

We have used PM6 semi-empirical method in the Gaussian 09 program package to preliminarily optimize hydrogen bond complexes formed by A and small molecules (H_2O, CH_3OH, C_2H_5OH and CH_2O) [41]. The structure of the lowest energy has been chosen, further optimization and excited energy were calculated at PBE/TZVP level in the Turbomole 6.4 program package. In addition, electronic configurations were calculated at PBE/TZP level in the ADF 2010 program package [42-44].

The binding energies of hydrogen bond complexes have been calculated at PBE/TZVP level in the Turbomole 6.4 program package. The basis set superposition error (BSSE) can be corrected for using the counterpoise (CP) method. The original counterpoise method of Boys and Bernardi is the procedure most frequently used for computing the BSSE [45].

The binding energies of hydrogen bonds were performed by the following expression:

$$E_{binding} = E_{AB} - E_A - E_B \ , \tag{1}$$

In this case, the corrected $E_{binding}^{CP}$ is given by:

$$E_{binding}^{CP} = E_{AB} - E_{A(B)} - E_{B(A)} \ , \tag{2}$$

Where parentheses denote ghost basis sets without electrons or nuclear charges.

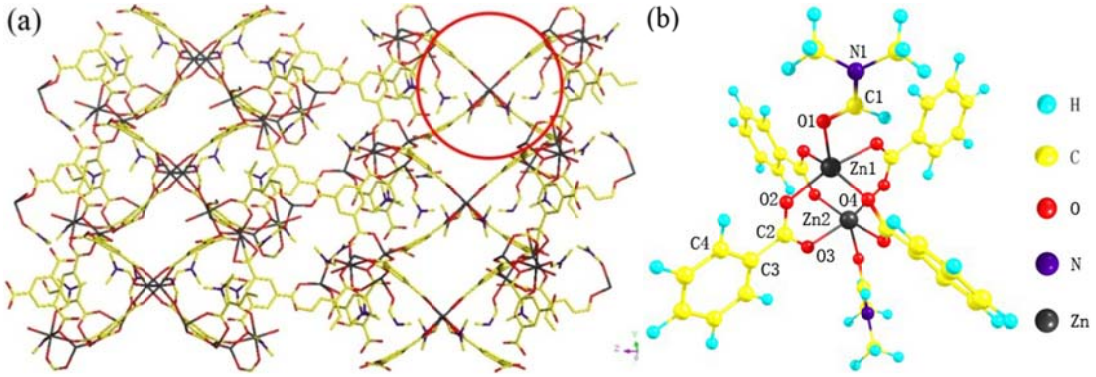

Figure 1: (a) crystal structure of $Zn_3(BTC)_2(DMF)_3(H_2O)\bullet(DMF)(H_2O)$ without H atoms. (b) Representative fragment of the $Zn_2L_4(DMF)_2$ structure optimized at PBE/ TZVP level.

3. Numerical Results and discussion

3.1 Ground-state geometric conformation, vibration frequency and UV-VIS maximum absorption peak of representative segment A

We have optimized the structure of representative segment A using PBE, B3LYP and CAM-B3LYP functional. The calculated results were compared to experimental structural properties (see **Table 1**). We also have calculated the vibration frequency and UV-VIS maximum absorption peak of A (see **Table 2**). In **Table 1** and **Table 2**, it can be seen that the results of the PBE level are in good agreement with experimental data. But the calculated dihedral angles and UV-VIS maximum absorption peak of B3LYP and CAM-B3LYP level are unsatisfactory with experimental data.

The optimized structure of A at PBE/TZVP level is showed in **Figure 1**(**b**). The representative segment A consists of two Zn atoms in the center, four benzoic acids around the two Zn atoms, and two N,N'-dimethylformamide (DMF) respectively connected to one Zn atom. In **Table 1**, we can see that the bond angle O2-Zn1-O4 is close to 90^{o} and this proves that four benzoic acids are evenly around the two zinc atoms. The dihedral angles O2-C2-C3-C4 near 0^{o} shows that benzoic acid keeps good co-planarity in the process of optimization.

Table 1 Selected bond lengths (Å), bond angles (^{o}), and dihedral angles (^{o}) of this MOFs optimized at PBE, B3LYP and CAM-B3LYP functional

	Exp	PBE	B3LYP	CAM-B3LYP
Zn1-Zn2	2.96	2.84	2.95	3.06
Zn1-O2	1.98	2.05	2.05	2.04
O2-C2	1.24	1.25	1.24	1.24
C1-N1	1.29	1.35	1.34	1.33
Zn1-O1-C1	118.49	117.47	118.73	117.99
O2-C2-O3	125.11	125.92	125.51	125.04
O2-Zn1-O4	87.05	86.28	85.66	87.48
Zn1-O2-O3-Zn2	3.93	4.52	13.53	0.61
O2-C2-C3-C4	0.01	1.28	1.34	2.33

3.2 Structures and bind energies of hydrogen bond complexes

There are many hydrogen bond donors and acceptors on the representative fragment of the A. Small molecules (H_2O, CH_3OH, C_2H_5OH and CH_2O) were allowed to adsorb in all

possible adsorption sites on the representative fragment. Considering the cost of calculation, a semi-empirical method was used for making preliminary optimization structure and the lowest energy complex of each small molecule-A complexes was picked out. Then the preliminary optimized structures were further optimized (see **Figure 2**) and the binding energies (see **Table 3**) of the lowest energy complexes were calculated at PBE/TZVP level.

Table 2 Compared vibration frequency (cm^{-1}) and UV-VIS maximum absorption peak (nm) of A from experimental measurements and our calculations

	Exp	PBE	B3LYP	CAM-B3LYP
vibration frequency				
C-H stretch	2931	2960	3025	3074
C=O stretch	1658/1628	1659/1625	1673/1615	1727/1667
Organic benzene ring breathing	1574/1442	1573/1434	1588/1417	1558/1482
C-N stretch	1257/1103	1239/1085	1269/1121	1313/1141
Zn-O stretch	571/540	567/535	573/550	577/560
UV-VIS maximum absorption peak	341	345	246	216

All the small molecules form hydrogen bonds with A. Hydrogen bond complexes H_2O-A, CH_3OH-A and C_2H_5OH-A have two hydrogen bonds, the strong one is O···H-O between the O atom of benzoic acid and the H atom of hydroxyl. But CH_2O-A only has a weak hydrogen bond between the O atom of benzoic acid and the H atom of CH2O. Presented in **Table3**, one can find that hydrogen bonds of CH_3OH-A and C_2H_5OH-A are very similar.

Table 3 BSSE corrected binding energies ($KJ \bullet mol^{-1}$) and calculated hydrogen bond lengths (Å) of the hydrogen bond complexes, O···H-O is the strong hydrogen bond and O′···H′ is the weak one.

	$E_{binding}^{CP}$	O···H-O	O′···H′
H_2O-A	-44.38	1.91	2.3
CH_3OH-A	-47.28	1.86	2.43
C_2H_5OH-A	-47.28	1.82	2.43
CH_2O-A	-31.84	--	2.57

To evaluate the adsorption behaviors of each small molecule, we calculated binding energies ($E_{binding}^{CP}$) of the different complexes with consideration of BSSE (see **Table 3**). The binding energies of H_2O-A, CH_3OH-A and C_2H_5OH-A are close, even it of CH_3OH-A is equal to C_2H_5OH-A. That demonstrates the hydrogen bonds of CH_3OH-A and C_2H_5OH-A

are essentially the same. The binding energy values of H_2O-A, CH_3OH-A, C_2H_5OH-A and CH_2O-A are -44.38, -47.28, -47.28 and -31.84 KJ mol-1, respectively. This proves that A has good adsorption behaviors for these small molecules by hydrogen bond.

3.3 electronic transition and frontier molecular orbitals of hydrogen bond complexes

The electronic excitation energies and the oscillation strengths of the low-lying electronically excited states for the A and its hydrogen bond complexes were calculated using the TDDFT method and were presented in **Table 4** for comparison. Zhao *et al.* has demonstrated for the first time that hydrogen bond strengthening can lower the excitation energy of a related excited state and therefore induce electronic spectral redshift, and that hydrogen bond weakening can increase the excitation energy of a related excited state and hence electronic spectral blueshift occurs [24]. According to the above rules, we predicted the excited-state hydrogen bond strengthening or weakening behavior by monitoring changes in the excitation energy. It is obvious that the electronic excitation energy of CH_3OH-A and CH_2O-A could induce a redshift compared with A. This indicates that hydrogen bonds are strengthened for the excited states. However, blueshift of excitation energy occurs to other complexes. That is to say, the increase of the energy levels of the excited states induced by hydrogen bonding would be weaker than those of the ground state.

Table 4 Calculated electronic excitation energies (eV) and corresponding oscillator strengths (in parentheses) of the low-lying electronically excited states for A, H_2O-A, CH_3OH-A, C_2H_5OH-A and CH_2O-A. The orbital transition contributions for the singlet electronic excited states are also listed (R: redshift, B: blueshift, H: HOMO, L: LUMO).

	A	H_2O-A	CH_3OH-A	C_2H_5OH-A	CH_2O-A
S1	3.609(0.965E-3) H→L，99.8%	3.629(0.432E-3)B H→L，99.8%	3.577(0.537E-3)R H→L，94.6%	3.659(0.873E-3)B H→L，99.8%	3.469(0.715E-3)R H→L，99.1%
S2	3.695(0.124E-2)	3.746(0.500E-2)B	3.618(0.243E-3)R	3.744(0.862E-3)B	3.561(0.166E-2)R
S3	3.742(0.513E-2)	3.762(0.487E-2)B	3.709(0.986E-3)R	3.769(0.441E-2)B	3.674(0.968E-3)R
S4	3.767(0.442E-2)	3.784(0.990E-3)B	3.739(0.299E-2)R	3.851(0.370E-4)B	3.728(0.772E-3)R
S5	3.824(0.119E-2)	3.885(0.118E-2)B	3.743(0.307E-2)R	3.853(0.301E-3)B	3.775(0.148E-2)R
S6	3.850(0.297E-3)	3.897(0.158E-3)B	3.776(0.244E-2)R	3.881(0.568E-2)B	3.786(0.444E-2)R

The oscillator strength of A in the S3 state is the largest among the low-lying excited

states and it is different in H_2O-A, CH_3OH-A, C_2H_5OH-A and CH_2O-A, namely S_2, S_5, S_6, S_6, respectively. Kasha's rule states that photon emission occurs in appreciable yields only from the lowest excited state of a given multiplicity. Because the radiationless transition from the S_n ($n>1$) state to the S1 state is ultrafast, we just discuss the properties of A and its hydrogen bond complexes in the S1 state here. It is obvious that the contribution to S_1 is from the highest occupied molecular orbital (HOMO) to the lowest unoccupied molecular orbital (LUMO), so we have studied charge transfer using frontier molecular orbitals (FMOs) and the electronic configurations (see in **Figure 3**).

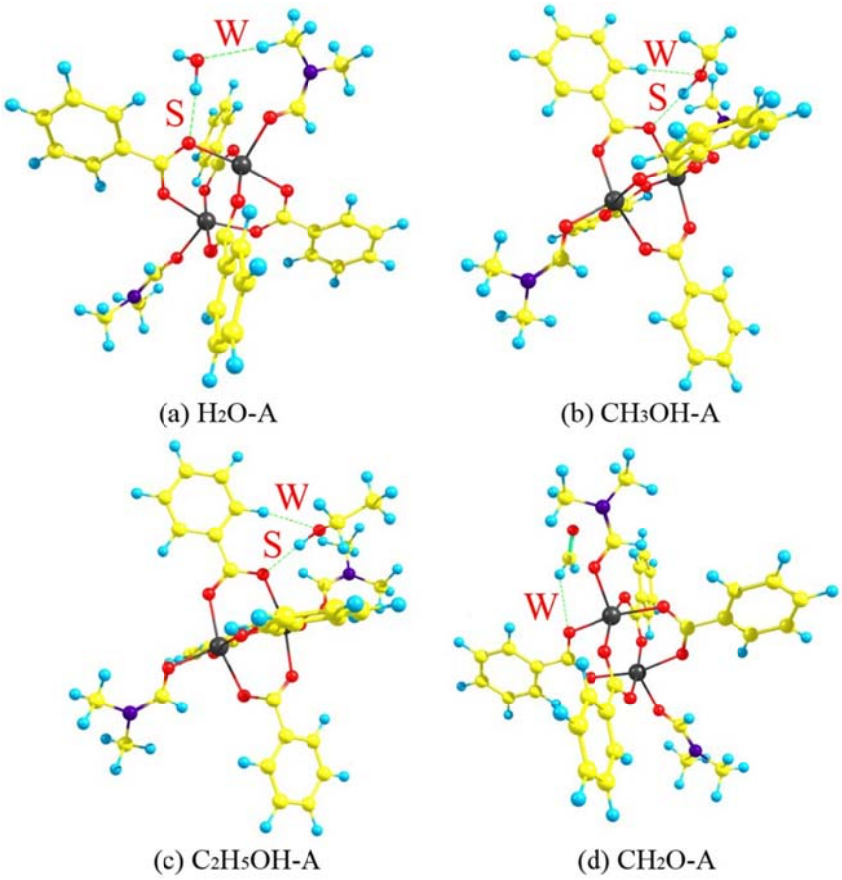

Figure 2: Geometric structures of the hydrogen bond complexes, (a) H_2O-A, (b) CH_3OH-A, (c) C_2H_5OH-A, (d) CH_2O-A and the hydrogen bonds illustration (S: strong hydrogen bond, W: weak hydrogen bond)

Figure 3(**a**) shows the FMOs of A, the electron densities of HOMO are localized on a carboxyl moiety and the electron densities of LUMO are localized on a L moiety. The corresponding electronic configurations can further evidence that HOMO and LUMO are mainly composed of n orbitals of O atoms and π^* orbitals of C atoms, respectively. It is

evident that the S_1 state has n-π^* character. We can find out that the origin of luminescence is dominated by the direct organic ligands excitation. The FMOs of H_2O-A and C_2H_5OH-A are displayed in **Figure 3**(**b**) and 3(d), respectively. The HOMO and LUMO of are also mostly composed of n orbitals of O atoms onto the carboxyl and π^* orbitals of C atoms onto the benzene ring. We have already conjectured that the hydrogen bonding would be weakened in the corresponding electronic excited state. So the electron densities of L will be increased in the S_1 state, this can facilitate the intermolecular electron transfer (ET) in the S_1 states and result in the fluorescence quenching. **Figure 3**(**c**) shows the HOMO of CH_3OH-A is mainly composed of n orbitals of O atoms onto carboxyl and CH_3OH, and the LUMO of CH_3OH-A

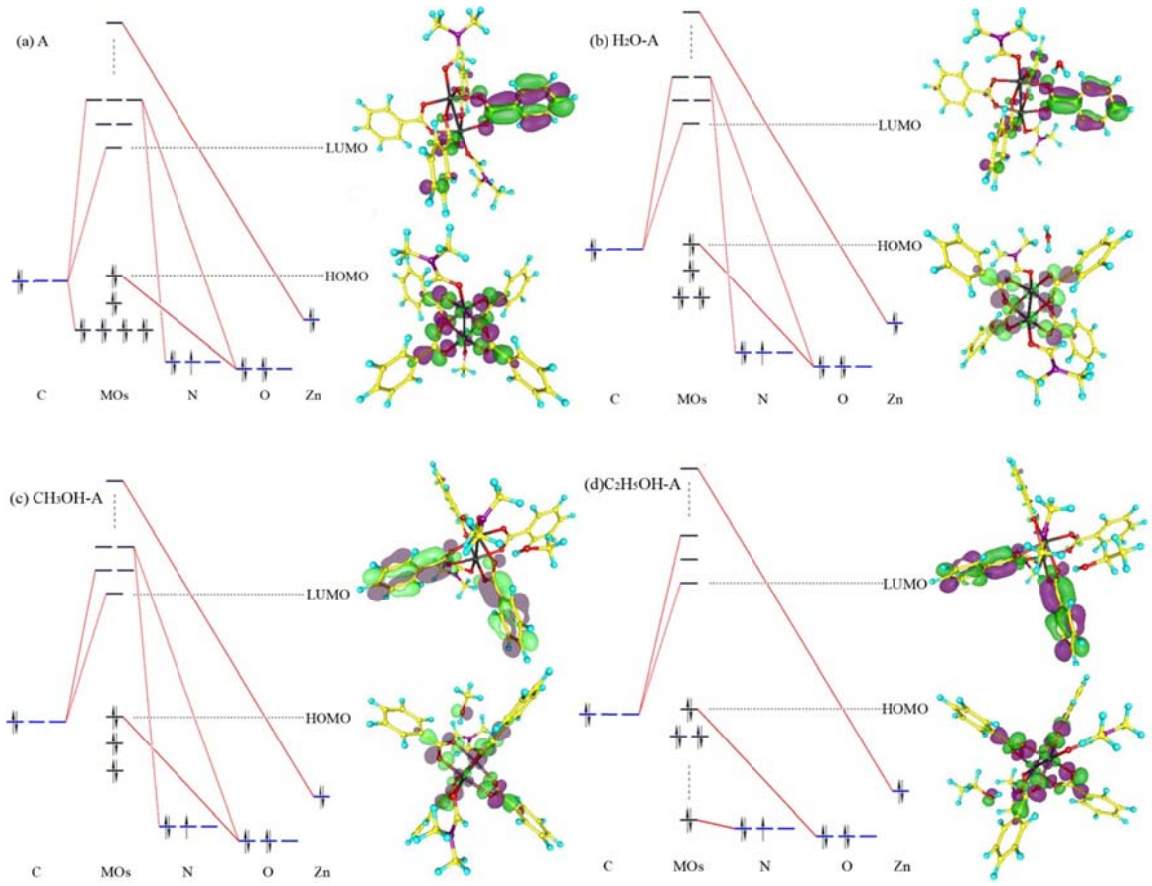

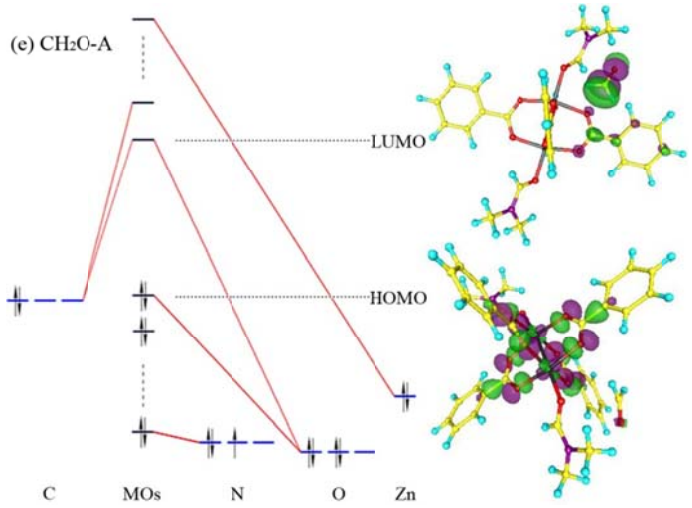

Figure 3: Calculated frontier molecular orbitals (FMOs) and the corresponding electronic configurations of (a) A, (b) H_2O-A, (c) CH_3OH-A, (d) C_2H_5OH-A and (e) CH_2O-A.

is mostly constituted by π* orbitals of C atoms onto the benzene ring. The hydrogen bonding of H_2O-A would be strengthened in the corresponding electronic excited state. The electron densities of L will be decreased in the S_1 state, and the distance between the O atoms and L increases the path length of the ET. Both above will result in ET weakening. So the fluorescence will be enhanced. However, the FMOs of CH_2O-A displayed in **Figure 3**(**e**) have some difference from any one of them above. Although the HOMO is still mostly composed of n orbitals of O atoms onto the carboxyl, the LUMO is mainly constituted by π* orbitals of C and O atoms onto the CH_2O. The electron densities of LUMO are localized on the CH_2O moiety. The origin of luminescence has been changed into being dominated by the guest-induced luminescence. So the luminescent functional MOFs will be a chemical sensor for detecting formaldehyde.

4. Conclusion

In this work, DFT and TDDFT method are employed to investigate the adsorption behaviors and the luminescence property of the representative fragment A of $Zn_3(BTC)_2(DMF)_3(H_2O)\bullet(DMF)(H_2O)$. The result of the tests of different functional and base sets illustrates that PBE function and TZVP basis sets are good for simulating A. The BSSE corrected binding energies of the hydrogen bond complexes (H_2O-A, CH_3OH-A, C_2H_5OH-A and CH_2O-A) prove that A shows good adsorption behaviors for these small molecules by hydrogen bonds. The FMOs and the corresponding electronic configurations of A obviously

show that the origin of luminescence is dominated by the direct organic ligands excitation. The electronic excitation energies of C_2H_5OH-A and H_2O-A are blueshift compared with A, so the hydrogen bonds of them are weaker than those of the ground state. Fluorescence quenching will occur for the facilitating intermolecular ET in the S_1 states. On the contrary, the electronic excitation energies of CH_3OH-A and CH_2O-A are redshift compared with A, so the hydrogen bonds of them are strengthened for the excited states. The intermolecular ET of CH_3OH-A is weakened in the S_1 states will result in fluorescence enhancement. However, the electron densities of LUMO of CH_2O-A are localized on the CH_2O moiety. The origin of the MOFs luminescence is changed into dominating by the guest-induced luminescence. As a result, the functional MOFs have good adsorption behaviors and excellent luminescence property. Furthermore, small molecules can be adsorbed and change the luminescence property, especially CH_2O changes its origin of luminescence. So it will be a probe for detecting small molecules. Particularly, the MOFs will be used to detect formaldehyde in environment.

Acknowledgments

Support of this work by the National Natural Science Foundation of China (Grants 21036006, 21137001) and the Dalian Scientific Program (No. 2011A15GX023) is gratefully acknowledged.

References

[1] M. Yaghi, M. O'Keeffe, N. W. Ockwig, H. K. Chae, M. Eddaoudi, J. Kim, Reticular synthesis and the design of new materials, Nature, 423 (2003), 705-714.

[2] H. X. Deng, C. J. Doonan, H. Furukawa, R. B. Ferreira, J. Towne, C. B. Knobler, B. Wang, O. M. Yaghi, Multiple functional groups of varying ratios in metal-organic frameworks, Science, 327 (2010), 846-850.

[3] N. Stock, S. Biswas, Synthesis of Metal-Organic Frameworks (MOFs): Routes to Various MOF Topologies, Morphologies, and Composites, Chem. Rev., 112 (2012), 933-969.

[4] D. J. Tranchemontagne, J. L. Mendoza-Cortes, M. O'Keeffe, O. M. Yaghi, Secondary building units, nets and bonding in the chemistry of metal–organic frameworks, Chem. Soc. Rev., 38 (2009), 1257-1283.

[5] S. Kitagawa, R. Kitaura, S. Noro, Functional Porous Coordination Polymers, Angew. Chem. Int. Ed., 43 (2004), 2334-2375.

[6] H. Khajavi, J. Gascon, J. M. Schins, L. D. A. Siebbeles, F. Kapteijn, Unraveling the Optoelectronic and Photochemical Behavior of Zn_4O-Based Metal Organic Frameworks, J. Phys. Chem. C, 115 (2011), 12487-12493.

[7] M. Guo, H. L. Cai, R. G. Xiong, Ferroelectric metal organic framework, Inorg. Chem. Commun., 13

(2010), 1590-1598.

[8] J. R. Li, R. J. Kuppler, H. C. Zhou, Selective gas adsorption and separation in metal–organic frameworks, Chem. Soc. Rev., 38 (2009), 1477-1504.

[9] M. D. Allendorf, C. A. Bauer, R. K. Bhakta, R. J. T. Houk, Luminescent metal-organic frameworks, Chem. Soc. Rev., 38 (2009), 1330-1352.

[10] S. T. Meek, J. A. Greathouse, M. D. Allendorf, Metal-Organic Frameworks: A Rapidly Growing Class of Versatile Nanoporous Materials, Adv. Mater., 23 (2011), 249-267.

[11] Y. J. Cui, Y. F. Yue, G. D. Qian, B. L. Chen, Luminescent Functional Metal-Organic Frameworks, Chem. Rev., 112 (2012), 1126-1162.

[12] L. E. Kreno, K. Leong, O. K. Farha, M. Allendorf, R. P. Van Duyne, J. T. Hupp, Metal-Organic Framework Materials as Chemical Sensors, Chem. Rev., 112 (2012), 1105-1125.

[13] H. M. Bolt, G. H. Degen, J. G. Hengstler, The carcinogenicity debate on formaldehyde: how to derivesafe exposure limits? Arch. Toxicol., 84 (2010) 421-422.

[14] L. R. Rhomberg, L. A. Bailey, J. E. Goodman, A. K. Hamade, D. Mayfield, Is exposure to formaldehyde in air causally associated with leukemia? A hypothesis based weight of evidence analysis, Crit. Rev. Toxicol., 41 (2011), 555-621.

[15] A. Duong, C. Steinmaus, C. M. McHale, C. P. Vaughan, L. P. Zhang, Reproductive and developmental toxicity of formaldehyde: a systematic review, Mut. Res., 728 (2011), 118-138.

[16] R. Golden, Identifying an indoor air exposure limit for formaldehyde considering both irritation and cancer hazards, Crit. Rev. Toxicol., 41(2011), 672-721.

[17] K. H. Kim, S. A. Jahan, J. T. Lee, Exposure to formaldehyde and its potential human health hazards, Carcinog. Ecotoxicol. Rev., 29 (2011), 277-299.

[18] P. R. Chung, C. T. Tzeng, M. T. Ke, C. Y. Lee, Formaldehyde Gas Sensors: A Review, Sensors, 13 (2013), 4468-4484.

[19] G. J. Zhao, K. L. Han, Early time hydrogen-bonding dynamics of photoexcited coumarin 102 in hydrogen-donating solvents: theoretical study, J. Phys. Chem. A, 111(2007), 2469-2474.

[20] C. Y. Lv, L. J. Sun, B. Q. Wang, C. Y. Zhang, J. Zhang, A TD-DFT Study on Fluorescent Chemosensor for Fluoride Anion Based on Dipyrrolyl Derivatives, Commun. Comput. Chem, 1 (2013), 282-296.

[21] G. J. Zhao, K. L. Han, Ultrafast hydrongen-bonding dynamics of photoexcited coumarin 102 in hydrogen-donating solvents: theoretical study, J. Phys. Chem. A, 111 (2007), 9218–9223.

[22] G. J. Zhao, K. L. Han, Role of Intramolecular and Intermolecular Hydrogen Bonding in Both Singlet and Triplet Excited States of Aminofluorenones on Internal Conversion, Intersystem Crossing, and Twisted Intramolecular Charge Transfer, J. Phys. Chem. A, 113 (2009), 14329-14335.

[23] G. J. Zhao, K. L. Han, Effects of hydrogen bonding on tuning photochemistry: Concerted hydrogen-bond strengthening and weakening, ChemPhysChem, 9(2008), 1842-1846.

[24] G. J. Zhao, J. Y. Liu, L. C. Zhou, K. L. Han, Site-selective photoinduced electron transfer from alcoholic solvents to the chromophore facilitated by hydrogen bonding: A new fluorescence

quenching mechanism, J. Phys. Chem. B, 111 (2007), 8940-8945.

[25] G. J. Zhao, K. L. Han, Site-Specific Solvation of the Photoexcited Protochlorophyllide a in Methanol: Formation of the Hydrogen-Bonded Intermediate State Induced by Hydrogen-Bond Strengthening, Biophysical Journal, 94 (2008), 38-46.

[26] Y. Zhao, D. G. Truhlar, Density functionals with broad applicability in chemistry, Acc. Chem. Res., 41 (2008), 157–167.

[27] G. J. Zhao, K. L. Han, Time-dependent density functional theory study on hydrogen-bonded intramolecular charge-transfer excited state of 4-dimethylamino-benzonitrile in methanol, J. Comput. Chem., 29 (2008), 2010-2017.

[28] M. Majumder, T. Goswami, A. Misra, S. Bardhan, S. K. Saha, Intermolecular Interaction in 2-Aminopyridine: A Density Functional Study, Commun. Comput. Chem, 1 (2013), 225-234.

[29] M. Z. Zhang, B. P. Ren, Y. Wang, C. X. Zhao, Excited-state Intramolecular Proton Transfer of HDI and HBF: Excited-state Hydrogen-bonding Dynamics and Electronic Structures, Commun. Comput. Chem, 1 (2013), 216-224.

[30] Y. H. Liu, S. C. Lan, Polarity Effect of Solvents on Ground- and Excited-state Hydrogen Bonds, Commun. Comput. Chem, 1 (2013), 235-243.

[31] G. J. Zhao, K. L. Han, pH-Controlled twisted intramolecular charge transfer (TICT) excited state via changing the charge transfer direction, Phys. Chem. Chem. Phys., 12 (2010), 8914-8918.

[32] G. J. Zhao, K. L. Han, Hydrogen bonding in the excited states, Acc. Chem. Res., 45 (2012), 404-413.

[33] J. J. Tan, C. Hao, N. N. Wei, M. X. Zhang, X. Y. Dai, Time-Dependent Density Functional Theory Study on the Electronic Excited-State Hydrogen Bonding Dynamics of Methyl Acetate in Aqueous Solution, Theor. Comput. Chem., 10 (2011), 393-400.

[34] Q. R. Fang, G. S. Zhu, M. Xue, J. Y. Sun, F. X. Sun, S. L. Qiu, Structure, uminescence, and adsorption properties of two chiral microporous metal-organic frameworks, Inorg. Chem., 45 (2006), 3582-3587.

[35] J. P. Perdew, Y. Wang, Accurate and simple analytic representation of the electron-gas correlation energy, Phys. Rev. B, 45 (1992), 13244-13249.

[36] A. D. Becke, Density-Functional Thermochemistry. III. The Role of Exact Exchange, J. Chem. Phys., 98 (1993), 5648-5652.

[37] R. Ahlrichs, M. Bar, M. Haser, H. Horn, C. Kolmel, Electronic structure calculations on workstation computers: The program system Turbomole, Chem. Phys. Lett., 162 (1989), 165-169.

[38] A. Schafer, C. Huber, R. Ahlrichs, Fully optimized contracted Gaussian-basis sets of Triple Zeta Valence Quality for Atoms Li to Kr, J. Chem. Phys., 100 (1994), 5829-5835.

[39] T. Yanai, D. Tew, N. Handy, A new hybrid exchange-correlation functional using the Coulomb-Attenuating Method (CAM-B3LYP), Chem. Phys. Lett., 393 (2004), 51-57.

[40] M. J. Frisch, G. W. Trucks, H. B. Schlegel, G. E. Scuseria, M. A. Robb, J. R. Cheeseman, G. Scalmani, V. Barone, B. Mennucci, G. A. Petersson, H. Nakatsuji, M. Caricato, X. Li, H. P. Hratchian, A. F. Izmaylov, J. Bloino, G. Zheng, J. L. Sonnenberg, M. Hada, M. Ehara, K. Toyota, R. Fukuda, J. Hasegawa, M.

Ishida, T. Nakajima, Y. Honda, O. Kitao, H. Nakai, T. Vreven, J. A. Jr. Montgomery, J. E. Peralta, F. Ogliaro, M. Bearpark, J. J. Heyd, E. Brothers, K. N. Kudin, V. N. Staroverov, T. Keith, R.Kobayashi, J. Normand, K. Raghavachari, A. Rendell, J. C. Burant, S. S. Iyengar, J. Tomasi, M. Cossi, N. Rega, J. M. Millam, M. Klene, J. E. Knox, J. B. Cross, V. Bakken, C. Adamo, J. Jaramillo, R. Gomperts, R. E. Stratmann, O. Yazyev, A. J. Austin, R. Cammi, C. Pomelli, J. W. Ochterski, R. L. Martin, K. Morokuma, V. G. Zakrzewski, G. A. Voth, P. Salvador, J. J. Dannenberg, S. Dapprich, A. D. Daniels, O. Farkas, J. B. Foresman, J. V. Ortiz, J. Cioslowski, D. J. Fox, Gaussian 09, Revision B.01, Gaussian, Inc., Wallingford CT, 2010.

[41] J. J. P. Stewart, A G4MP2 theoretical study on the gas phase enthalpies of formation for various polycyclic aromatic hydrocarbons (PAHs) and other C_{10}through C_{20} unsaturated hydrocarbons, J. Mol. Model., 13 (2007), 1173-1213.

[42] E. Van Lenthe, E. J. Baerends, Optimized Slater-type basis sets for the elements 1-118, J. Comput. Chem., 24 (2003), 1142-1156.

[43] G. te Velde, F. M. Bickelhaupt, E. J. Baerends, C. F. Guerra, S. J. A. Van Gisbergen, J. G. Snijders, T. Ziegler, Chemistry with ADF, J. Comput. Chem., 22 (2001), 931-967.

[44] ADF2010, SCM, Theoretical Chemistry, Vrije Universiteit, Amsterdam, The Netherlands, E. J. Baerends, T. Ziegler, J. Autschbach, D. Bashford, A. Bérces, F. M. Bickelhaupt, C. Bo, P. M. Boerrigter, L. Cavallo, D. P. Chong, L. Deng, R. M. Dickson, D. E. Ellis, M. van Faassen, L. Fan, T. H. Fischer, C. Fonseca Guerra, A. Ghysels, A. Giammona, S. J. A. van Gisbergen, A. W. Götz, J. A. Groeneveld, O. V. Gritsenko, M. Grüning, S. Gusarov, F. E. Harris, P. van den Hoek, C. R. Jacob, H. Jacobsen, L. Jensen, J. W. Kaminski, G. van Kessel, F. Kootstra, A. Kovalenko, M. V. Krykunov, E. van Lenthe, D. A. McCormack, A. Michalak, M. Mitoraj, J. Neugebauer, V. P. Nicu, L. Noodleman, V. P. Osinga, S. Patchkovskii, P. H. T. Philipsen, D. Post, C. C. Pye, W. Ravenek, J. I. Rodríguez, P. Ros, P. R. T. Schipper, G. Schreckenbach, J. S. Seldenthuis, M. Seth, J. G. Snijders, M. Solà, M. Swart, D. Swerhone, G. te Velde, P. Vernooijs, L. Versluis, L. Visscher, O. Visser, F. Wang, T. A. Wesolowski, E. M. van Wezenbeek, G. Wiesenekker, S. K. Wolff, T. K. Woo, A. L. Yakovlev.

[45] S. F. Boys, F. Bernardi The calculation of small molecular interactions by the differences of separate total energies. Some procedures with reduced errors, Mol. Phys., 19 (1970), 553–566.